Millimeter-resolution acousto-optic quantitative imaging in a tissue model system

Aliaksandr Bratchenia
University of Twente
Institute of Biomedical Technology
Faculty of Science and Technology
P.O. Box 217
7500 AE Enschede
The Netherlands
E-mail: a.bratchenia@tnw.utwente.nl

Robert Molenaar
University of Twente
Institute of Biomedical Technology
Faculty of Science and Technology
P.O. Box 217
7500 AE Enschede
The Netherlands

Ton G. van Leeuwen
University of Twente
Institute of Biomedical Technology
Faculty of Science and Technology
P.O Box 217
7500 AE Enschede
The Netherlands
and
University of Amsterdam
Academic Medical Center
Biomedical Engineering and Physics
P.O. Box 22700
1100 DE Amsterdam
The Netherlands

Rob P. H. Kooyman
University of Twente
Institute of Biomedical Technology
Faculty of Science and Technology
P.O. Box 217
7500 AE Enschede
The Netherlands

Abstract. We have investigated the application of ultrasound modulated coherent light for quantitative determination of the ratio of dye concentrations and total concentration of absorbers in a blood vessel–mimicking sample. A 3-mm-diam tube containing the mixture of dyes inside an Intralipid-based gel with optical properties similar to tissue was interrogated by two different laser wavelengths in combination with intense microsecond ultrasound bursts. The use of calibration curves allowed us to extract quantitative information on the ratio of dye concentrations with the accuracy of better than 15%, as well as on the total concentration. Furthermore, we demonstrated the feasibility to obtain a quantitative 3-D map of the absorbing structure with a spatial resolution of better than 3 mm. These findings give an outlook to apply this technique for noninvasive 3-D mapping of oxygen saturation and total concentration of hemoglobin in tissue. [DOI: 10.1117/1.3153894]

Keywords: acousto-optics; coherent optical systems; tissues; speckle interferometry; spectrometry.

Paper 08449R received Dec. 18, 2008; revised manuscript received Apr. 16, 2009; accepted for publication Apr. 16, 2009; published online Jun. 23, 2009; corrected Jul. 9, 2009.

1 Introduction

An instrument that can noninvasively quantify parameters as total hemoglobin concentration and oxygen saturation locally and deep in tissue would have numerous applications in clinical medicine. Pulse oximetry, which is a standard technique for oxygenation measurements, has certain limitations connected with a low perfusion state.[1] Moreover, it is not applicable for localized measurements deep in tissue. Diffuse optical tomography can measure deep within tissue, but the resolution decreases severely with increasing depth.[2] One way to overcome this difficulty is to combine optics with ultrasound (US) as is done in photoacoustic[3] and acousto-optic (AO) imaging.[4–8] It has been shown that photoacoustics has the capability to provide quantitative data on local absorbances[9–11], but a mathematical model is always required to estimate the local fluence. In AO, the local fluence can be measured in a more direct manner because, at the site(s) of interest, the local light intensity is acoustically labeled. In this paper, we investigate the feasibility to apply AO for millimeter-resolution measurements of the ratios of concentrations of optical absorbers in a model system mimicking a blood vessel embedded in tissue at different positions.

Generally, the major interest to AO was given with respect to its *qualitative* imaging abilities;[12–14] only recently the use of AO for *quantitative* purposes was demonstrated in model systems.[15–17] Kim et al.[16] were the first to show that estimation of the total concentration and the concentration ratio of

Address all correspondence to Aliaksandr Bratchenia, BioPhysical Engineering (BPE), Faculty of Science and Technology, University of Twente, P.O. Box 217-Enschede, Overijssel 7500AE Netherlands; Tel: +31534893112; Fax: +31534891105; E-mail: a.bratchenia@tnw.utwente.nl

1083-3668/2009/14(3)/034031/6/$25.00 © 2009 SPIE

two dyes in nonscattering inclusions embedded in tissue phantoms was feasible by irradiating the sample at two optical wavelengths. However, the utilized semi-continuous wave (semi-cw) US (2-ms bursts) did not allow one to have an US-axial spatial resolution better than the length of US focal zone (~20 mm).[18] Thus, in order to have noticeable changes of the measured signal with changes of the absorption coefficient of the inclusion, the cylindrical inclusion was positioned parallel to the US burst propagation direction. The use of nonscattering absorbing inclusions, without a cladding, allowed them to approximate the optical pathlength through the absorber by the diameter of that object and thus to directly apply the Beer–Lambert law for the dependence of the amplitude of the measured signal on the local optical absorption coefficient.

Previously, we have shown that the use of microsecond US bursts combined with a gated optical excitation enabled the measurement of the absorption coefficient of an embedded dye in a scattering solution with a high spatial resolution.[17] Consequently, the absorbing cylinder can be positioned *perpendicularly* to both the light path and the US path, which results in a more practical geometry for *in vivo* measurements.

In this paper, we extend our approach to multiple wavelengths and try to determine the concentration ratio of one component to the other and total concentration of a bicomponent absorber inside a silicone rubber tube placed in an Intralipid (IL)-based phantom. We first calibrated the instrument by measuring the experimental response to the known absorption coefficient of a single-component absorber embedded in the scattering phantom. The response to a single-component absorber with the absorption coefficient equal to that of the surrounding medium was taken as a baseline. Experimental data were normalized to this baseline and fitted to a Lambert–Beer-type model. Subsequently, we used the obtained fitting coefficients to determine the absorption coefficient from measured data for an unknown bicomponent absorber. With these established absorption coefficients and the molar extinction coefficients for pure dye components, which are known for each wavelength, we can calculate the fraction of a single component in the mixture of absorbers and the total concentration of these absorbers. In addition, we demonstrate the feasibility to measure a 3-D absorption map of the phantom.

2 Materials and Methods

The phantoms used in the experiments were based on an IL solution incorporated in an Agar matrix ($\mu_s' \approx 1.5$ mm^{-1}, similar to the reduced scattering coefficient of tissue) filled into Perspex containers (*XYZ* dimensions $\sim 15 \times 45 \times 40$ mm^3 or $20 \times 45 \times 40$ mm^3). US-absorbing material was placed on the bottom of the container. For the phantom with a width of 15 mm, a single silicone rubber tube (3 mm i.d., similar to the size of a human artery) was mounted in the center of the container with its axis along the *Y*-axis (cf. Fig. 1). There is an acoustical impedance mismatch between the used silicone rubber (~1 MRayl), and the IL-Agarose phantom material (~1.5 MRayl). This causes slight distortions in the measured AO signal when US is falling at highly oblique angles on the tube walls; however, the used data treatment technique (see below) cancels out these slight distortions. For the phantom with a width of 20 mm, three parallel vessels,

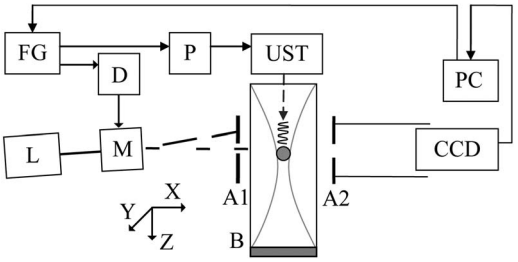

Fig. 1 Schematics of the acousto-optical setup in transmission geometry. FG: two-channel programmable function generator (Tektronix AFG3102). D: delay line. P: MOSFET pulser to drive transducer. UST: 2.25 MHz US transducer (Panametrics V306). L: He–Ne laser, 35 mW at 633 nm and Argon-Ion laser, 260 mW at 514 nm. M: acousto optical modulator (Isomet 1201E-1). A1: aperture to block non-deflected light. A2: aperture for speckle selection system. B: IL-based phantom. CCD: camera. In the center of the phantom the cross-section of an absorber containing tube is depicted. The US-propagation is along the *Z* direction.

with a mutual distance of ~5 mm, were mounted perpendicularly to the optical axis in the center of the phantom. Each tube contained the same IL mixed with ink of a predefined absorbance. For the calibration procedure, two types of ink absorbers (Ecoline) were used, with their absorption maximum at $\lambda = 513$ nm and $\lambda = 608$ nm. To mimic the saturation values of oxy-hemoglobin, a set of absorbers was prepared by mixing IL with the two types of inks in 11 linearly changing ratios: 0:100, 10:90, …, 90:10, 100:0.

The experimental setup, as shown in Fig. 1 and described in Ref. 17, was extended to a two-wavelengths system. High-pressure (~1.5 MPa) US bursts of ~1 μs length, which were produced by a 2.25-MHz transducer with a focal zone length of ~16 mm and a focal zone width of <2 mm, were transmitted along the *Z*-axis at 30-kHz repetition rate. At the position of the absorbing material, this short US pulse resulted in an effective US disturbance volume of $\sim 2 \times 2 \times 3$ mm^3 in *XYZ* dimensions. Laser light pulses of ~1 μs length were created by deflection of a cw He–Ne laser beam (633 nm, 35 mW) or a cw argon ion laser beam (514 nm, 260 mW) by an acousto-optical modulator and delayed in the range of 5–25 μs relative to the start of the US burst. These pulses, which illuminated the tissue-mimicking phantom along the *X*-axis, produced a speckle pattern, which was detected by a CCD camera (Basler A102f, 12 bits, 1392×1040 pixels). The camera and a 6-mm diaphragm were positioned such that approximately one speckle illuminated one pixel.[19] Laser beam, diaphragm, and camera axis were positioned approximately in line. In order to rule out as much as possible environmental effects, such as vibrations, which could disturb the speckle pattern, the camera exposure time was chosen to be as short as possible. Within a camera exposure time of ~80 ms, several hundreds of light/US pulse cycles were accumulated to yield one image with a signal-to-noise ration (SNR) sufficient for determination of the mean pixel intensity and its standard deviation. These two parameters, which for each probed position of the US burst averaged over 16 images, were used for further processing. The measurements were performed sequentially for each wavelength.

The analysis of the images was performed in the same way as in Ref. 17. In short, the AO-induced image contrast change

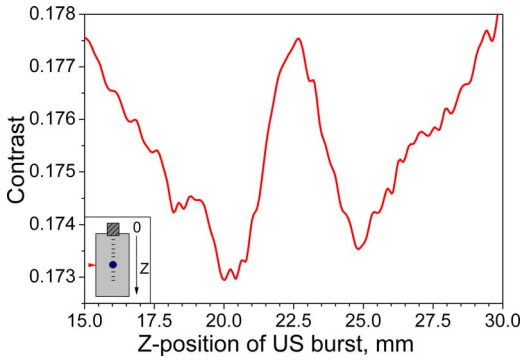

Fig. 2 Dependence of contrast profile on the *Z*-axis position of US burst in the presence of an absorber at $z \approx 22.5$ mm. The width of the absorber is ≈3 mm. Contrast profile is spline interpolated.

ΔC as detected by a CCD camera can be used as a measure for the fraction of light absorbed in the AO probed volume.[13] For each absorbance, we measured a contrast profile $C=C(z)$, where z is the position of the US packet.[17] An example of such an experimentally determined profile is given in Fig. 2. From this curve, we estimate a spatial resolution of better than 3 mm, as judged from the full width at half maximum of the contrast curve around $z \approx 22.5$ mm. From these profiles, we determined the modulation depth M at the position where the US packet is within the tube ($z \approx 22.5$ mm). M, defined here as the ratio of US modulated to unmodulated light intensity, can be determined:[13]

$$M(z) = \frac{\Delta C(z)}{C(z)}, \tag{1a}$$

where $\Delta C = C_b\ C$, C_b is the background contrast value determined when the US was "off," and C is the contrast value in the region of interest.

The SNR of the system is determined by the detected light intensity and the ratio of modulated light intensity over unmodulated intensity. Thus, in order to have a measure of the quality of the measured profile, we introduce the maximum SNR of $M(z)$, which is defined in the following way:

$$\mathrm{SNR}_{\max} = \frac{M_{\max}}{\sigma_{M_{\max}}} \tag{1b}$$

where $M_{\max}$ is the maximum M in a given profile of measured modulation depth values and $\sigma_{M_{\max}}$ is the standard deviation of $M_{\max}$, which is obtained from the standard deviation σ_C of corresponding contrast values. From Fig. 2, which is a typical raw result from a measurement it can be estimated that $\sigma_C < 10^{-4}$.

In our experiments, SNR varied between 16 and 96, mainly depending on the light intensity that was measured. For a typical contrast value $C=0.2$, we estimate $\sigma_{M_{\max}} \approx 5 \times 10^{-4}$.

It has been shown[17] that, if the positions and sizes of the absorbing zone and US focus remain constant throughout the experiments, then changes in M correspond to the change of the photon flux through the US pressure zone in the absorbing structure. However, the value of M is dependent not only on local acousto-optical properties of a medium in the modulation zone but also on the local photon density in that zone and on the optical pathlength that modulated photons need to travel to the detector. In order to account for these M variations, we tentatively introduce the normalized modulation depth $\bar{M}$

$$\bar{M}(\vec{r},\lambda) = \frac{M(\vec{r},\lambda)}{M_{\mu_a=0}(\vec{r},\lambda)}, \tag{2}$$

where M is the modulation depth measured in the presence of an absorber in the US modulation zone, $M_{\mu_a=0}$ is the M measured in the absence of the absorber, and $\vec{r}$ is the position of the center of the US modulation zone.

In order to investigate the dependence of $\bar{M}(\lambda)$ from the absorber's position within the phantom, we used the triple-vessel phantom. By moving the US transducer along the *X*-axis, the AO effect was measured for a wavelength of 514 nm and a 2-D map of M values in the *XZ* plane was built, both for the situations where each vessel contained no absorber and where the absorber ($\mu_a \approx 0.27\ \mathrm{mm}^{-1}$ or $\mu_a \approx 0.54\ \mathrm{mm}^{-1}$) was present. From these 2-D maps, only those M that correspond to $z \approx 22.5$ mm (*Z*-axis position of centers of vessels) were taken and considered further.

For calibration of the instrument, the experimental response of the single-vessel phantom to a known range of absorption coefficients was measured for both wavelengths. Experimental data were fitted to a Lambert–Beer type model,

$$\bar{M}(\lambda) = \bar{M}_0(\lambda) * e^{-\Delta\mu_{\mathrm{ext}}(\lambda)*l_{\mathrm{eff}}(\lambda)} + \bar{M}_{\mathrm{bgd}}(\lambda), \tag{3}$$

with the following fitting coefficients: l_{eff} is the average of lightpaths through the US modulation zone and $\bar{M}_{\mathrm{bgd}}(\lambda)$ is the normalized background modulation depth caused by residual US disturbances outside the absorbing structure. In view of the rather short US bursts that we used, shear waves contribute only marginally to $\bar{M}_{\mathrm{bgd}}(\lambda)$.

$\bar{M}_0(\lambda) = (1 - \bar{M}_{\mathrm{bgd}})$ is the normalized modulation depth in the absence of the absorber originating from the vessel only, and $\Delta\mu_{\mathrm{ext}}$ is the difference in extinction coefficients of the US-interrogated volume and the environment. Because in our experiments the scattering coefficient remained constant, we can replace the change of the extinction coefficient in the US modulation zone just by the change of the absorption coefficient: $\Delta\mu_{\mathrm{ext}} = \Delta\mu_a$. The parameter $\bar{M}_{\mathrm{bgd}}(\lambda)$ can be measured in the situation when the vessel contains an absorber with a very high absorption coefficient. The parameter l_{eff} was also estimated using a Monte Carlo software package[17] that had the option to follow the path of photons traversing the US-irradiated zone.

To determine the absorption coefficient for a range of unknown bicomponent absorbers, which imitate different states of oxygen saturation in a blood vessel, we devised the following procedure: Each measured value of modulation depth was normalized to the reference modulation depth according to Eq. (2). Absorption coefficients were calculated from Eq. (3) using the values for the model parameters obtained in the calibration procedure.

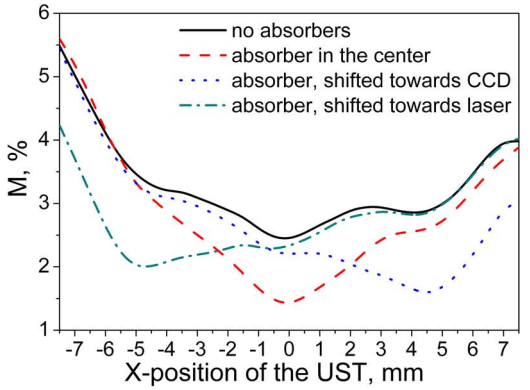

(a)

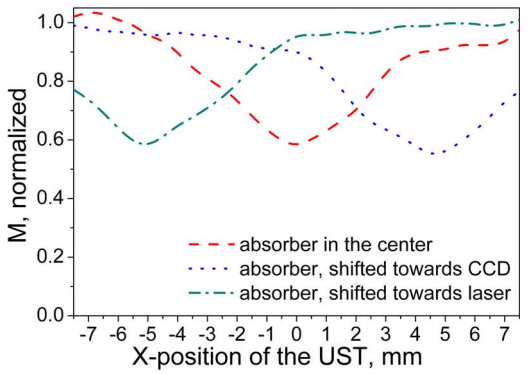

(b)

Fig. 3 Modulation depth as a function of the position of the US transducer in the three vessel phantom. μ_a of absorbers was 0.27 mm^{-1} for $\lambda=514$ nm. (a) Measured modulation depth and (b) modulation depth, normalized to the reference.

From the obtained μ_a values for different wavelengths, we can calculate the total concentration X_{total} and S, which is the fraction of X_1 in the mixture,

$$X_{total}=[X_1]+[X_2]=\frac{\mu_a(\lambda_1)\Delta\varepsilon_1(\lambda_2)-\mu_a(\lambda_2)\Delta\varepsilon_1(\lambda_1)}{\varepsilon_1(\lambda_1)\varepsilon_2(\lambda_2)-\varepsilon_1(\lambda_2)\varepsilon_2(\lambda_1)} \quad (4)$$

$$S=\frac{[X_1]}{[X_1]+[X_2]}=\frac{\mu_a(\lambda_2)\varepsilon_1(\lambda_1)-\mu_a(\lambda_1)\varepsilon_1(\lambda_2)}{\mu_a(\lambda_1)\Delta\varepsilon(\lambda_2)-\mu_a(\lambda_2)\Delta\varepsilon(\lambda_1)} \quad (5)$$

where $\mu_a(\lambda)$ (in mm^{-1}) is the absorption coefficient for the corresponding wavelength; $\varepsilon_1(\lambda)$ and $\varepsilon_2(\lambda)$ are the known absorption coefficients (mm^{-1}) of the two types of ink stock solutions; $\Delta\varepsilon(\lambda)=\varepsilon_1(\lambda)-\varepsilon_2(\lambda)$; and $[X_1]$ and $[X_2]$ are the concentrations of the two absorbers.

3 Results and Discussion

First, we experimentally demonstrated that, for a single absorber in the homogeneous scattering medium, $\bar{M}(\lambda)$ is independent from the absorber's position within the phantom. The results of these experiments for the absorber with $\mu_a\approx0.27$ mm^{-1} are shown in Fig. 3(a). By application of Eq. (2), we can construct $\bar{M}$, which is depicted in Fig. 4 for the various positions of the absorbing US-interrogated vessels.

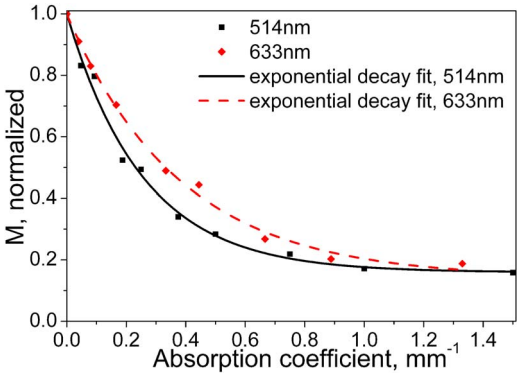

Fig. 4 Calibration curves for each wavelength in the single-vessel phantom.

Figure 3(b) shows that $\bar{M}$ remains constant for the three positions of the absorbing vessel. For various experiments using different phantoms, this result was repeatedly found. Similar results were obtained for the case where $\mu_a\approx0.54$ mm^{-1} (data not shown).

Before we carried on with the calibration procedure, the response was tested for a system consisting of an absorbing vessel with $\mu_a\approx0.415$ mm^{-1} and a surrounding phantom material with $\mu_a'\approx0.015$ mm^{-1}. It was found, not surprisingly, that the measured M was the same as that resulting from a situation where $\Delta\mu_a=\mu_a-\mu_a'$ remains constant, but with $\mu_a\approx0.400$ mm^{-1} and $\mu_a'\approx0$. In view of the available laser power, in further experiments we used phantoms with $\mu_a'\approx0$.

In Fig. 4, $\bar{M}$'s used for calibration are depicted as a function of inclusions with known μ_a. From Fig. 4, we can see that at $\mu_a>\sim0.8$ mm^{-1} the modulation depth remains approximately constant because the light is almost completely absorbed within the modulation zone inside the vessel. For a set absorption coefficient $\mu_a(\lambda)$, we can apply a Lambert–Beer-type model [Eq. (3)] to the data depicted in Fig. 4 and obtain fitting coefficients for the model. Effective pathlengths were found to be ~3.9 mm for $\lambda=514$ nm and ~2.8 mm for $\lambda=633$ nm and are in a good agreement with those obtained from Monte Carlo calculations[20] (~3.8 mm for $\lambda=514$ nm and ~3.1 mm for $\lambda=633$ nm).

After the calibration of the instrument, we performed measurements with the set of bicomponent absorbers. An example of the resolved absorption coefficients (for $\lambda=514$ nm) is given in Fig. 5. With these established absorption coefficients and the molar extinction coefficients for pure dye components, which are known for each wavelength, we calculated the fraction S of a single component in the mixture of absorbers (and the total concentration of these absorbers). The result of this calculation is presented in Fig. 6. From the graph, we see that within the error bars the measured fraction of X_1 in the mixture is in line with theoretical expectations. In the range that is equivalent to the physiological range of saturation (50–100%) the accuracy of the measured S is ~15%. Furthermore, within a margin of error of ~20%, the total concentration of the two absorbing dyes was measured to be the expected 100%, as seen in Fig. 7.

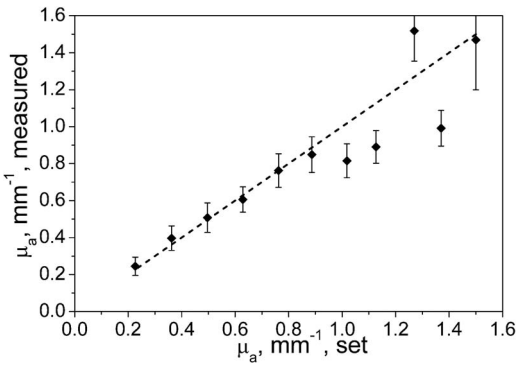

Fig. 5 Measured absorption coefficients for the set of bicomponent absorbers for λ = 514 nm in the single-vessel phantom. The dotted line corresponds to a perfect match between set and measured absorption coefficient.

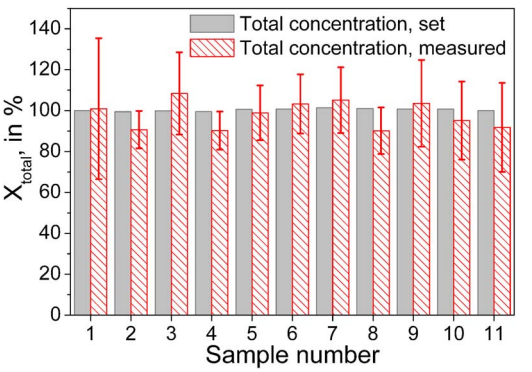

Fig. 7 X_{total}, the total concentration of the mixture, both for experimental and set data for the various prepared absorber combinations in the single-vessel phantom. The linearly changing ratios (100:0, 90:10,…, 10:90, 0:100) are denoted as the sample numbers: 1, 2,…, 10, 11, respectively.

4 Implications and Limitations

The most striking result of our study is that the use of normalized modulation depth and calibration curves, measured for each of the wavelengths at a single point, allowed us to establish a quantitative correlation between local absorbances in the phantom and the measured signal at any position within the phantom (cf. Fig. 3–5) as well as to obtain information on the ratios of dye concentrations inside the tube (cf. Fig. 6).

Using the same procedure, it is possible to expand the proposed technique and to perform 3-D mapping of the phantom by moving the US transducer in the lateral XY plane. To demonstrate this, we built up a $\bar{M}$ value map of the three vessel phantom, with the two outer vessels filled with absorbing dye. The cross section of this map (along the X-axis) is shown in Fig. 8. From the plot we clearly see the location of the tubes and their shadows. The spatial resolution was determined from the full width at half maxima of the contrast curves (cf. Fig. 2) of the absorbing objects measured in the various directions and was found to be ~2 mm in the axial Z direction, ~4 mm in the lateral X direction. The resolution in the lateral Y direction could not be determined due to the geometry of the phantom but is expected to be similar to that in the X direction.

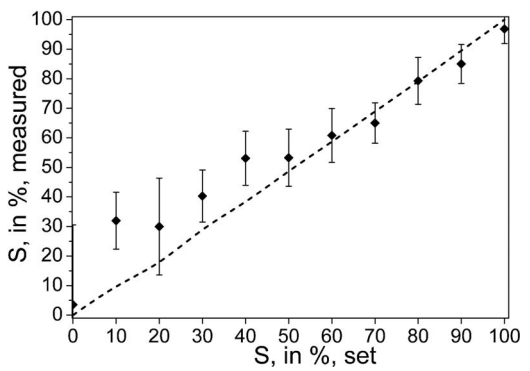

Fig. 6 S, the fraction of X_1 in the mixture, for the various prepared absorber combinations in dependence of set data in the single-vessel phantom. The dotted line corresponds to a perfect match between set and measured S.

The major limitation of the proposed method is the normalization procedure, in which a set of measured modulation depth values M in the absence of absorbing inhomogeneities has to be measured. However, if it is not possible to perform the measurement of M in the absence of these inhomogeneities, the baseline M can be obtained numerically (e.g., by

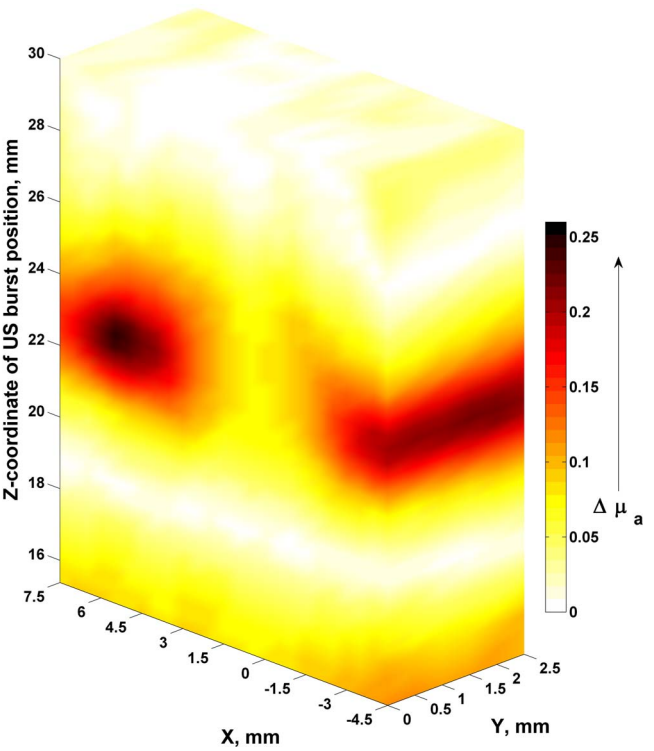

Fig. 8 The X-axis cross section of the map of $\Delta\mu_a \in [0;0.26]$ values. X, Y are the coordinates of the US transducer. Light is entering the phantom from the right. The outer vessels within the phantom contain the absorbing dye. The figure was constructed from datasets containing 186 Z-scans which took ~286 min to complete. Scanning step size: 0.375 mm in the Z direction and 0.5 mm in the X-Y directions. Scanning range: 35 mm in the Z direction, 15 mm in X direction and 2.5 mm in the Y direction. For these data, the maximum SNR is ~96.

Monte Carlo methods or by solving the diffusion approximation for the radiative transfer equation with finite element method).

The significant discrepancy of the measured data with the theoretical expectation at high absorbance values (Fig. 5) is due to the flatness of the calibration curve in this range of absorbances: small variations in the detected M result in large variations of μ_a. This implies that there is only a limited useful range over which μ_a can be determined. For the current phantom geometry with the employed optical and US power, this range can be quoted as

$$\mu_a l_{\text{eff}} \equiv \varepsilon_a[X] l_{\text{eff}} \sim < 4. \quad (6)$$

Of course, for a known extinction coefficient $\varepsilon_a(\lambda)$, the range of detectable concentrations can be adjusted by selecting an appropriate laser wavelength.

Another limitation is in the employed equipment. The phantom used in this study had a speckle decorrelation time τ_s of ~1 s. In living tissue τ_s varies between ~100 μs (blood in vessels with ~2-mm diam) and a few milliseconds (muscle tissue). In the detection approach as described in Sec. 2, it is essential that during one exposure time of the camera (in this study 80 ms) the speckle pattern remains stationary. Hence, with the current combination of light source and detection method, it will be difficult to repeat these measurements in living tissue. However, using a more powerful light source and a holographic detection scheme,[21] preliminary experiments that we have done point to a usable exposure time on the order of ~50 μs, bringing quantitative measurements in living tissue within reach.

5 Conclusion

In conclusion, we have shown that acousto-optics can be used for quantitative characterization of bicomponent absorbers in a phantom resembling a tissue-embedded blood vessel. The obtained spatial resolution is better than 3 mm. The used calibration technique allowed us to measure $\Delta\mu_a$ irrespective of the position of the absorber along the X-axis. The extension of this technique to measurements of $\Delta\mu_a$ anywhere in a phantom and for a phantom of any width is straightforward, provided a map of $M_{\mu_a=0}$ is available for the region of interest. The further development of this approach could lead to the introduction of functional AO tomography.

A difficulty that has to be resolved before functional AO can be applied to living tissue is the detection of an AO-induced modulation depth in the presence of fast speckle decorrelation. We expect that the use of a shot-noise limited holographic detection scheme[21] that takes advantage of a heterodyne amplification factor,[22] together with a more powerful light source will overcome this problem and that AO can be used for millimeter-resolution 3-D monitoring of, e.g., the oxygenation state of living tissue.

Acknowledgments

We thank Dr. P. Brands (ESAOTE) for help with the US instrumentation. This research was supported by the Technical Science Foundation of The Netherlands (STW) Project No. TGT.6656.

References

1. A. Jubran, "Pulse oximetry," *Crit. Care* **3**(2), R11–R17 (1999).
2. J. Ripoll, M. Nieto-Vesperinas, and R. Carminat, "Spatial resolution of diffuse photon density waves," *J. Opt. Soc. Am. A* **16**(6), 1466–1477 (1999).
3. X. Wang, Y. Pang, G. Ku, X. Xie, G. Stoica, and L.-H. V. Wang, "Non-invasive laser-induced photoacoustic tomography for structural and functional imaging of the brain *in vivo*," *Nat. Biotechnol.* **21**, 803–806 (2003).
4. L.-H. Wang, S. L. Jacques, and X.-M. Zhao, "Continuous-wave ultrasonic modulation of scattered laser light to image objects in turbid media," *Opt. Lett.* **20**(6), 629–631 (1995).
5. W. Leutz and G. Maret, "Ultrasonic modulation of multiply scattered light," *Physica B* **204**, 14–19 (1995).
6. M. Kempe, M. Larionov, D. Zaslavski, and A. Z. Genack, "Acousto-optic tomography with multiply scattered light," *J. Opt. Soc. Am. A* **14**(5), 1151–1158 (1997).
7. L.-H. V. Wang, "Mechanisms of ultrasonic modulation of multiply scattered coherent light: an analytic model," *Phys. Rev. Lett.* **87**(4), 043903 (2001).
8. E. Granot, A. Lev, Z. Kotler, and B. G. Sfez, "Detection of inhomogeneities with ultrasound tagging of light," *J. Opt. Soc. Am. A* **18**(8), 1962–1967 (2001).
9. L. Yin, Q. Wang, Q. Zhang, and H. Jiang, "Tomographic imaging of absolute optical absorption coefficient in turbid media using combined photoacoustic and diffusing light measurements," *Opt. Lett.* **32**(17), 2556–2558 (2006).
10. B. T. Cox, S. R. Arridge, K. P. Kostli, and P. C. Beard, "Two-dimensional quantitative photoacoustic image reconstruction of absorption distributions in scattering media by use of a simple iterative method," *Appl. Opt.* **45**(8), 1866–1875 (2006).
11. J. Laufer, D. Delpy, C. Elwell, and P. Beard, "Quantitative spatially resolved measurement of tissue chromophore concentrations using photoacoustic spectroscopy: application to the measurement of blood oxygenation and haemoglobin concentration," *Phys. Med. Biol.* **52**(1), 141–168 (2007).
12. S. Leveque, A. C. Boccara, M. Lebec, and H. Saint-Jalmes, "Ultrasonic tagging of photon paths in scattering media: parallel speckle modulation processing," *Opt. Lett.* **24**(3), 181–183 (1999).
13. J. Li, G. Ku, and L.-H. V. Wang, "Ultrasound-modulated optical tomography of biological tissue by use of contrast of laser speckles," *Appl. Opt.* **41**(28), 6030–6035 (2002).
14. C. Kim, R. J. Zemp, and L.-H. V. Wang, "Intense acoustic bursts as a signal-enhancement mechanism in ultrasound-modulated optical tomography," *Opt. Lett.* **31**(16), 2423–2425 (2006).
15. R. P. H. Kooyman and C. Loccioni, "Acousto-optic spectroscopy as a tool for non-invasive determination of chemical compounds in blood: a feasibility study," *Proc. SPIE* **5702**, 39–43 (2005).
16. C. Kim and L.-H. V. Wang, "Multi-optical-wavelength ultrasound-modulated optical tomography: a phantom study," *Opt. Lett.* **32**(16), 2285–2287 (2007).
17. A. Bratchenia, R. Molenaar, and R. P. H. Kooyman, "Feasibility of quantitative determination of local optical absorbances in tissue-mimicking phantoms using acousto-optic sensing," *Appl. Phys. Lett.* **92**, 113901 (2008).
18. A. Bratchenia, R. Molenaar, and R. P. H. Kooyman, "Acousto-optic spectroscopy as a tool for quantitative determination of chemical compounds in tissue: a model study," *Proc. SPIE* **6437**, 64371P (2007).
19. J. W. Goodman, "Statistical properties of laser speckle patterns," in *Laser Speckle and Related Phenomena*, J. C. Dainty, Ed., Chap. 2, Springer-Verlag, Berlin, (1984).
20. F. F. M. de Mul, M. H. Koelink, M. L. Kok, P. J. Harmsma, J. Greve, R. Graaff, and J. G. Aarnoudse, "Laser Doppler velocimetry and Monte Carlo simulations on models for blood perfusion in tissue," *Appl. Opt.* **34**(28), 6595–6611 (1995).
21. M. Atlan, B. C. Forget, F. Ramaz, and A. C. Boccara, "Pulsed acousto-optic imaging in dynamic scattering media with heterodyne parallel speckle detection," *Opt. Lett.* **30**(11), 1360–1362 (2005).
22. B. J. Berne and R. Pecora, *Dynamic Light Scattering*, Wiley, Hoboken, NJ (1976).